Exchange and fine-structure effects in autoionization of large-angular-momentum doubly excited Rydberg states

Michel Poirier
Commissariat à l'Energie Atomique, Service "Photons, Atomes et Molécules," Centre d'Etudes de Saclay, 91191 Gif-sur-Yvette, France
(Received 1 April 1994)

Autoionization probabilities of doubly excited atoms with one electron in a large-l Rydberg state are investigated through first-order perturbation theory in a single-configuration approach. In the framework of the jk-coupling scheme, the formalism takes into account multipoles higher than dipoles in the electronic interaction and exchange effects. Exchange effects are computed using the Froese method for Slater integrals and are demonstrated to be significant as long as $l < 5$. The essential importance of fine-structure transitions when the outer electron is in a large-l state is emphasized. Comparison with available experimental data shows that Slater integrals are reliably computed and that fair agreement is generally obtained for g states, while even strongly autoionizing f states are at least qualitatively represented. Correlation effects may explain some remaining disagreement with the measured autoionization widths.

PACS number(s): 32.80.Dz, 31.50.+w

I. INTRODUCTION

The study of doubly excited autoionizing atoms and ions is an active field today both theoretically [1] and experimentally [2]. During the past decade, particular attention has been devoted to alkaline-earth atoms with an electron in a large-angular-momentum Rydberg state [3–9]. The reasons for that are multiple. Such levels appear as especially stable and therefore fall into the class of long-lived states in the continuum. They provide an ideal framework for theoretical computation: since the two active electrons are spatially separated, an *ab initio* treatment seems possible. Besides, a series of recent works has outlined the importance of *fine-structure transitions*. Using electron spectroscopy, Sandner *et al.* [10] have shown that the $6p_{3/2}ns_{1/2}$ $(J=1)$ states of barium, lying above the $6p_{1/2}$ threshold if $n>11$, autoionize at 60–70% towards this neighboring threshold. Accordingly, Kachru *et al.* [11] noticed an enhancement of $(6d_{5/2}nd_j)$ $J=4$ width for $n \geq 26$, i.e., above the $6d_{3/2}$ ionization limit of Ba^+. An analogous statement has been made for the $7p_{3/2}nd$ levels of barium by Pruvost *et al.* [12]. One may ask whether such behavior also holds for an outer electron in a large-l state. A clue in this sense is given by several observations. In barium, Bente and Hogervorst noticed that the scaled linewidths of one of the $5d_{5/2}nf$ $J=5$ series [13] and of the $6p_{3/2}nh$ series [7] dramatically increase when the fine-structure transition becomes allowed. Lastly, the strong difference in the autoionizing behavior of $5d_{5/2}nc$ (where nc means "circular state," $n=l+1$) and $5d_{3/2}nc$ observed by Roussel *et al.* [14] has been interpreted by considering the decay channel $5d_{5/2}nl \rightarrow 5d_{3/2}\varepsilon l'$. To account theoretically for such transitions, one has to consider the quadrupolar term in the electronic interaction. Since this term is of shorter range than the dipolar one, the usual approximation consisting in neglecting the wave-functions overlap is less valid [6]. One has then to consider exchange effects. From a general point of view, it is also interesting to provide a quantitative check of the "long-range" (i.e., without exchange) approximation generally used in describing large-l autoionization. As experimental evidence for exchange phenomena in autoionization, one may quote the fact that levels labeled in jk coupling with the same momentum k but different total momentum J may have different widths [15]. The influence of the multipolar contributions have been stressed recently both theoretically [16] and experimentally [17]; the effect of quadrupolar electronic interaction in the presence of static electric and magnetic fields has been analyzed recently by Chen *et al.* [18]. When considering higher doubly excited states such as the "double circular" $4f5g$ states [19], one may suspect that transitions of high multipolarity, for instance to the $7s$ limit, contribute significantly to the autoionization process.

In Sec. II of the present paper, we outline the basic formalism for the large-l autoionization process in alkaline-earth atoms including exchange in the jk-coupling framework. Section III is devoted to the numerical method for deriving Slater integrals involved in the autoionization probability. In Sec. IV we apply the formalism to the autoionization processes of large-l Rydberg states in barium or strontium and compare our results with some available experimental data in Sec. V. Concluding remarks are given in the last section.

II. AUTOIONIZATION FORMALISM FOR LARGE-l RYDBERG STATES

The basic formalism for the autoionization process of alkaline-earth atoms in large-l Rydberg states has been developed in several papers [5,6,20]. We outline here the improvements with respect to previous theories, putting emphasis on exchange effects, quadrupolar transitions, and spin-dependent effects.

We consider an atom with two active electrons. The outer electron is termed the *Rydberg electron* and its coordinates are referred through index 1. The inner electron is termed the *valence electron* and its coordinates are referred through index 2. One assumes that the outer electron weakly penetrates the valence orbit. The influence of the other electrons, referred to as *core electrons,* has been considered in a previous paper [5]. In the single-configuration description of autoionization adopted here, the Rydberg electron evolves from a bound hydrogenic state $(n_1 l_1)$ to a continuum state (εl) while the valence electron falls from the excited ionic state $(n_2 l_2 j_2)$ to a lower state $(n_0 l_0 j_0)$. Due to its small overlap with the core and the valence-electron orbit, the Rydberg electron may be described by Coulomb wave functions. Since this electron is assumed to be in a large-l state, its velocity is low and all relativistic effects concerning it may be ignored. Conversely, the valence-electron wave function, though still described in a monoelectronic formalism, accounts for core-polarization and core-penetration effects [21]; the singly ionized spectrum is represented as accurately as possible. As apparent from the above-mentioned quantum numbers, relativistic effects for this electron, i.e., spin, are included (e.g., spin-orbit splitting is 1700 cm^{-1} for the $6p$ state of Ba^+).

For the slow electrons considered here, the relativistic terms (Breit Hamiltonian) in the electronic interaction are quite negligible and the autoionization originates only in the $1/r_{12}$ term. Asymptotically, the Rydberg electron is subject to a potential $-(Z-1)/r_1$ (Z, net charge of the core, is 2 for alkaline-earth atoms, but isoelectronic sequences may also be considered through the present formalism). As in scattering theory, the additional interaction seen in the reaction zone is $1/r_{12}-1/r_1$. The Hamiltonian for two-electron atoms is written as (atomic units are used throughout)

$$H=H_0+V \ , \tag{2.1a}$$

$$H_0=\frac{p_1^2}{2}+\frac{p_2^2}{2}-\frac{Z}{r_2}-\frac{Z-1}{r_1} \ , \tag{2.1b}$$

$$V=\frac{1}{r_{12}}-\frac{1}{r_1} \ . \tag{2.1c}$$

In practically cases, the potential acting on electron 2 is not Z/r_2, as in (2.1b), but some more complex function describing the interaction with a nucleus surrounded by a closed-shell core; the details of this potential are not needed, provided one can get accurate enough eigenfunctions for this Hamiltonian; this point has been discussed in a previous paper [21]. Conversely, for the external electron the potential is indeed assumed to be $(Z-1)/r_1$, but the influence of the core polarized by the valence electron can also be accounted for [5].

Special attention has to be paid to the *coupling scheme* of angular momenta. This problem for one highly excited electron has been discussed by several authors [3,5,7,8,15]. The valence electron strongly interacts with the core; hence the spin-orbit effect for this electron dominates all other interactions considered here. Conversely, the electronic repulsion $1/r_{12}$ is generally stronger than spin-orbit effects for the Rydberg electron. Thus the best order in coupling angular momenta is the jk (or jl) coupling defined as $\{[(l_2 s_2)j_2 l_1]k s_1\}J$ [22]. Though the above description is not symmetric in the electron exchange, it can be shown [23] that perturbation theory can be applied in agreement with the Pauli principle, at least up to first order. The properly symmetrized wave function for the initial state is

$$|\Psi_i\rangle=2^{-1/2}[|\varphi_i(1,2)\rangle-|\varphi_i(2,1)\rangle] \ , \tag{2.2a}$$

where the unsymmetrized wave function for electrons (p,q) is

$$|\varphi_i(p,q)\rangle=|([q{:}n_2 l_2 j_2, p{:}n_1 l_1]k, p{:}s_1)JM\rangle \ . \tag{2.2b}$$

One assumes here, in agreement with the large-l hypothesis, that $l_1 \neq l_2$, so that $|\Psi_i\rangle$ is properly normalized. The final state is

$$|\Psi_f\rangle=2^{-1/2}[|\varphi_f(1,2)\rangle-|\varphi_f(2,1)\rangle] \tag{2.3a}$$

with

$$|\varphi_f(p,q)\rangle=|([q{:}n_0 l_0 j_0, p{:}\varepsilon l]k', p{:}s_1)J'M'\rangle \ . \tag{2.3b}$$

The autoionization probability will be derived from Fermi's golden rule. One has

$$\Gamma=2\pi|\mathcal{A}_d-\mathcal{A}_e|^2 \ , \tag{2.4a}$$

where the direct amplitude is

$$\mathcal{A}_d=\left\langle \varphi_f(1,2)\left|\frac{1}{r_{12}}-\frac{1}{r_1}\right|\varphi_i(1,2)\right\rangle \tag{2.4b}$$

and the exchange amplitude is

$$\mathcal{A}_e=\left\langle \varphi_f(2,1)\left|\frac{1}{r_{12}}\right|\varphi_i(1,2)\right\rangle \ . \tag{2.4c}$$

The total angular momentum (J,M) is conserved while, if exchange is included, the intermediate moment k may not be constant, at variance with the previous theory [5]. After recoupling of angular momenta, one gets for the direct amplitude in the jk scheme

$$\mathcal{A}_d=\delta_{JJ'}\delta_{MM'}\delta_{kk'}(-1)^{k-t-1/2}[l,l_1,l_0,l_2,j_0,j_2]^{1/2}\sum_{t\geq 0}\begin{pmatrix} l & t & l_1 \\ 0 & 0 & 0\end{pmatrix}\begin{pmatrix} l_0 & t & l_2 \\ 0 & 0 & 0\end{pmatrix}\begin{Bmatrix} l & t & l_1 \\ j_2 & k & j_0\end{Bmatrix}\begin{Bmatrix} l_0 & t & l_2 \\ j_2 & \frac{1}{2} & j_0\end{Bmatrix}$$
$$\times\langle n_0 l_0 j_0, \varepsilon l|r_<^t/r_>^{t+1}-\delta_{t0}/r_1|n_2 l_2 j_2, n_1 l_1\rangle \ , \tag{2.5}$$

with the notation

$$[a,b,\dots]=(2a+1)(2b+1)\dots \ . \tag{2.6}$$

The exchange amplitude is written as

$$\mathcal{A}_e=\delta_{JJ'}\delta_{MM'}\sum_{t\geq 0}\langle \epsilon l,n_0l_0j_0|r_<^t/r_>^{t+1}|n_2l_2j_2,n_1l_1\rangle U \ , \tag{2.7a}$$

with the angular part

$$U=[l,l_1,l_0,l_2,j_0,j_2,k,k']^{1/2}\begin{pmatrix} l & t & l_2 \\ 0 & 0 & 0 \end{pmatrix}\begin{pmatrix} l_0 & t & l_1 \\ 0 & 0 & 0 \end{pmatrix}(-1)^{J+t+1}\begin{bmatrix} \frac{1}{2} & l_2 & l & k' \\ j_2 & t & j_0 & J \\ k & l_1 & l_0 & \frac{1}{2} \end{bmatrix} . \tag{2.7b}$$

The last symbol of the angular factor is a $12j$ symbol of the second kind [24]. Details about its computation are given in the Appendix.

III. NUMERICAL METHOD

As developed in the preceding section, autoionization amplitudes involve angular factors and radial elements in the form of Slater integrals. The formulas for angular factors are developed in the Appendix. The method for computing Slater integrals is basically the one developed by Froese and other authors [25]. The present implementation of it allows one to account for core penetration and core polarization by the inner (or valence) electron because its wave function is a numerically derived wave function for the *parent* ion, describing as well as possible the interaction between core and valence electrons. The corresponding effects due to the Rydberg electron are almost negligible.

For the *exchange integral,* one writes

$$\langle \epsilon l,n_0l_0j_0|r_<^t/r_>^{t+1}|n_2l_2j_2,n_1l_1\rangle = \int_0^\infty dr_1 r_1 R_{n_0l_0j_0}(r_1)y^{(t)}(r_1)R_{n_1l_1}(r_1) \ , \tag{3.1a}$$

with

$$y^{(t)}(r_1)=r_1\int_0^\infty dr_2 r_2^2 R_{\epsilon l}(r_2)\frac{r_<^t}{r_>^{t+1}}R_{n_2l_2j_2}(r_2) \ . \tag{3.1b}$$

This function can be rewritten as

$$y^{(t)}(r_1)=(2t+1)\int_{r_1}^\infty dr_2 z^{(t)}(r_2)r_1^{t+1}\Big/r_2^{t+2} \ , \tag{3.2}$$

where the auxiliary function $z^{(t)}$ is given by

$$z^{(t)}(r_1)=\int_0^{r_1} dr_2 r_2^2 R_{\epsilon l}(r_2)(r_2/r_1)^t R_{n_2l_2j_2}(r_2) \ . \tag{3.3}$$

The numerical method for exchange integrals consists of five steps.

(i) The calculation of the bound radial wave functions of the parent ion $R_{n_il_ij_i}(r)$ taking into account core polarization; this step is performed by inward integration of the Schrödinger radial equation using spectroscopic energies and tabulated core size and polarizabilities [26] as developed in a previous paper [21]; core penetration can be estimated using an extrapolated form of the wave function [21].

(ii) The calculation of the continuum wave function $R_{\epsilon l}$: here the most numerically efficient method is also integration of the radial Schrödinger equation, which is stable when performed outwards because there is no classically forbidden outer region; normalization of this numerical function is done at the classical inner turning point where the analytic formulas developed by Seaton for the regular Coulomb wave function [27] are used together with a recursion relation on the l quantum number; the use of recursion relations may be necessary when Seaton's method is not accurate enough, i.e., when the turning point r (roughly proportional to l^2) is too large.

(iii) The calculation of the integral giving auxiliary function $z^{(t)}$.

(iv) The calculation of the bound Coulomb wave function $R_{n_1l_1}$; since the outer-electron wave function is assumed to be hydrogenic, this function is efficiently computed using the l downward recursion relation and analytic formulas to initiate it.

(v) The calculation of the $y^{(t)}$ function using the integral representation (3.2) and finally the calculation of the Slater integral using formula (3.1).

As in our previous work, radial integration is performed on a logarithmic mesh with an integration step usually taken as 10^{-3}. Since the valence-electron wave function has a small radial extension (assuming a low excitation $n_2l_2j_2$), the integration of $z^{(t)}(r_1)$ is performed on a domain small compared to the Rydberg wave-function extension. Assuming that the valence wave function cancels for r_1 greater than a certain r_M (a little larger than $2n_2^2$), beyond r_M the function $r_1^{t+1}z^{(t)}(r_1)$ is constant and, accordingly, the expression for $y^{(t)}$ is also very simple,

$$y^{(t)}(r_1)=\langle \epsilon l|r^t|n_2l_2j_2\rangle/r_1^t \quad \text{if } r_1>r_M \tag{3.4}$$

since the above matrix element is constant and factors out in the integral.

The *direct autoionization amplitude* was computed up to now using the nonpenetration approximation where $r_<^t/r_>^{t+1}$ is replaced by r_2^t/r_1^{t+1}. This approximation, together with discarding the exchange amplitude, is called hereafter the *long-range approximation.* Here we try to account for penetration and the long-range approx-

imation can be tested. To perform the integration, one decomposes the auxiliary function $z^{(t)}$ in an asymptotic part and a "short-range" part

$$z^{(t)}(r_1)=\int_0^{r_1} dr_2 r_2^2 R_{n_0 l_0 j_0}(r_2)(r_2/r_1)^t R_{n_2 l_2 j_2}(r_2) \quad (3.5a)$$

$$=\langle n_0 l_0 j_0|r^t|n_2 l_2 j_2\rangle \Big/ r_1^t-\zeta^{(t)}(r_1)\ , \quad (3.5b)$$

where $\langle n_0 l_0 j_0|r^t|n_2 l_2 j_2\rangle$ is a one-electron matrix element and $\zeta^{(t)}$ is the integral of the same functions as in $z^{(t)}$ but taken from r_1 to infinity. The interest of this decomposition is that the short-range part $\zeta^{(t)}(r_1)$ is zero for r_1 greater than the (usually small) spatial extension r_M of the *valence* electron wave functions $n_0 l_0 j_0$ and $n_2 l_2 j_2$. Without this decomposition one should have integrated (3.1) on a much larger interval, of the size of the *Rydberg* wave-function extension. Then one can exhibit in the direct Slater integral a factored contribution (up to now the only one considered) and an "exchange-type" contribution, as was done previously by Nikitin and Ostrovsky [20]. Namely, introducing the decomposition (3.5b) in the corresponding $y^{(t)}$ function, one gets the direct Slater integral

$$\langle \varepsilon l, n_0 l_0 j_0|r_<^t/r_>^{t+1}\ n_1 l_1, n_2 l_2 j_2\rangle=\langle n_0 l_0 j_0|r^t|n_2 l_2 j_2\rangle\langle \varepsilon l|r^{-t-1}|n_1 l_1\rangle$$
$$-(2t+1)\int_0^\infty dr_1 r_1^{t+2} R_{\varepsilon l}(r_1) R_{n_1 l_1}(r_1)\int_{r_1}^\infty dr_1' \zeta^{(t)}(r_1')\Big/ r_1'^{t+2}\ . \quad (3.6)$$

In the integral over r_1, the effective lower bound is a fraction of l^2, since closer to the origin the Rydberg wave functions are negligible, and the effective upper bound is the *valence* wave-function extension r_M since beyond r_M the short-range wave function $\zeta^{(t)}$ vanishes. So the second contribution to the direct integral involves (as is the case for the exchange integral) the overlap region between inner and outer wave functions, assumed to be small.

The comparison between the long-range part of the direct integral [first term of (3.6)] and either the exchange integral or the short-range part of the direct integral (3.6) defines numerically the validity of the long-range approximation. Some numerical values are given below.

The present method has been tested in various numerical cases. First, it can work properly even if the Rydberg final state is in the discrete spectrum instead of the continuum. Some numerical values listed by Butler, Minchin, and Wybourne [28] have been checked successfully. In the much more physically complex barium atom, the exchange integral $G^{(2)}(6p,15f)$ is computed to be 1.687×10^{-4} atomic units (a.u.) or 37.03 cm^{-1} for the $6p_{1/2}$ parent level and 1.838×10^{-4} a.u. or 40.33 cm^{-1} for the $6p_{3/2}$ level [according to the definition by Slater

TABLE I. Slater integrals for the $(6p_{3/2}24g)$ autoionization widths in barium. The integrals involved in the computation of the autoionization width of $6p_{3/2}24g[k]J$ states of barium are listed with respect to the final ionic state (threshold), angular l momentum of the ejected electron, and multipolarity order t. The direct integrals are the sum of the long-range part—where $r_<^t/r_>^{t+1}$ is replaced by r_2^t/r_1^{t+1}—and the short-range part.

	Exchange integrals			Direct integrals			
Threshold	l	t		l	t	Total	Long range	Short range
$6s_{1/2}$	3	4	3.248×10^{-4}	3	1	1.020×10^{-4}	2.159×10^{-4}	-1.139×10^{-4}
	5	4	1.600×10^{-4}	5	1	1.553×10^{-3}	1.578×10^{-3}	-2.480×10^{-5}
$5d_{3/2}$	1	2	-1.399×10^{-4}	3	1	1.196×10^{-4}	1.795×10^{-4}	-5.992×10^{-5}
	3	2	2.941×10^{-4}	5	1	1.273×10^{-3}	1.283×10^{-3}	-1.008×10^{-5}
	3	4	1.981×10^{-4}	1	3	-4.466×10^{-5}	2.600×10^{-5}	-7.066×10^{-5}
	5	4	7.164×10^{-5}	3	3	2.417×10^{-4}	4.260×10^{-4}	-1.842×10^{-4}
	5	6	5.292×10^{-5}	5	3	4.287×10^{-4}	4.561×10^{-4}	-2.748×10^{-5}
	7	6	6.891×10^{-6}	7	3	2.421×10^{-4}	2.441×10^{-4}	-2.003×10^{-6}
$5d_{5/2}$	1	2	-1.445×10^{-4}	3	1	1.295×10^{-4}	1.910×10^{-4}	-6.152×10^{-5}
	3	2	3.048×10^{-4}	5	1	1.348×10^{-3}	1.358×10^{-3}	-1.005×10^{-5}
	3	4	2.052×10^{-4}	1	3	-4.822×10^{-5}	2.623×10^{-5}	-7.445×10^{-5}
	5	4	7.173×10^{-5}	3	3	2.560×10^{-4}	4.450×10^{-4}	-1.890×10^{-4}
	5	6	5.298×10^{-5}	5	3	4.423×10^{-4}	4.696×10^{-4}	-2.737×10^{-5}
	7	6	6.650×10^{-6}	7	3	2.410×10^{-4}	2.430×10^{-4}	-1.927×10^{-6}
$6p_{1/2}$	2	3	6.110×10^{-4}	2	2	-3.907×10^{-4}	1.072×10^{-4}	-4.979×10^{-4}
	4	3	3.356×10^{-4}	4	2	2.647×10^{-3}	2.738×10^{-3}	-9.045×10^{-5}
	4	5	2.400×10^{-4}	6	2	3.355×10^{-4}	3.384×10^{-4}	-2.831×10^{-6}
	6	5	1.359×10^{-5}					

or Cowan [22], $G^{(k)}$ is twice the exchange integral (3.1) for the final state identical to the initial state]. Through a fine-structure splitting analysis, Abutaleb *et al.* [15] obtained 37 ± 2 cm^{-1} in unexpectedly good agreement with the present determination since the quantum defect of the nf states, of the order of 0.3, indicates that the Coulomb description for the outer electron is rather crude.

The Slater integrals involved in the computation of $(6p_{3/2}24g)$ states of barium are given in Table I. One can check that the largest values are obtained for the direct integrals $\langle 6s_{1/2}\varepsilon h|r_</r_>^2|6p_{3/2}24g\rangle$, $\langle 5d_j\varepsilon h|r_</r_>^2|6p_{3/2}24g\rangle$, and $\langle 6p_{1/2}\varepsilon g|r_</r_>^3|6p_{3/2}24g\rangle$. The dominant contribution among these three transitions will be determined for each couple of angular momenta k and J by their respective angular factors. The transitions to the $5d_j$ threshold are also possible through the octupolar effect ($t=3$), but according to Table I the corresponding Slater integrals are smaller, the same property holding when angular factors are included. The short-range contribution is negative in all the cases listed and usually tends to reduce the long-range value. For the highest l considered, physically the most important, the short-range term is a small correction; however, for lower l this term may be bigger than the long-range correction and thus reverse its sign. If final l is observed, i.e., if angular distributions are measured, the effect of short-range terms may be important. As a rule, the exchange radial integrals for g Rydberg states are smaller than direct integrals; taking angular factors into account, one also verifies that exchange effects are a rather small correction on the total autoionization width. However, the above statement about the contribution of the short-range direct integral to partial autoionization width (or angular distributions) also holds concerning exchange terms.

IV. APPLICATION TO ALKALINE-EARTH ATOMS AND DISCUSSION OF THE RESULTS

A. General trends

The above-discussed formalism has been applied to barium and strontium atoms for l_1 values ranging from 3 to 10. The autoionization probabilities of the $(6p_{3/2}24g)$ $[k=\frac{9}{2}]$ $J=5$ state of barium towards the different channels are detailed in Table II, where the results in the long-range approximation are also displayed. The dominant decay channel is $5d_{5/2}\varepsilon h$ but $6s_{1/2}\varepsilon h$ and $6p_{1/2}\varepsilon g$ contributions are not negligible; the $5d_{3/2}$ threshold is less favored because of angular factors and because the octupolar term reduces significantly the transition amplitude to $5d_{3/2}\varepsilon h$. One observes that some k-changing transitions ignored in the long-range approximation are present due to exchange effects, e.g., transition to $5d_{5/2}f$ $[k'=\frac{11}{2}]$, but they weakly contribute to the total width. From this table one concludes that long-range approximation gives good values for the total width while partial widths strongly depend on short-range effects.

The total widths of $6p_j24l_1[k]J$ states of barium for l_1 between 4 and 10 are listed in Table III. As was the case in the long-range approximation [5,20], one notices a strong decrease of the autoionization width versus the angular momentum l_1. For instance, for $l_1>6$ the autoionization lifetimes exceed 1 ns and are of the same magnitude order as or longer than radiative lifetimes. One less-noticed fact is that, for a given l_1, such probabilities are strongly dependent on the angular momentum k, since the widths range over more than three orders of magnitude if l_1 is 10. For example, in this case the computed lifetimes vary from 4.8 ns for $k=\frac{23}{2}$ to 8.7 μs for $k=\frac{17}{2}$. This statement stresses the necessity to define properly the angular-momentum coupling scheme. The jk-coupling scheme seems the more appropriate for high l_1; however, some departures from it may be observed for low l_1 [15]. One also observes that, due to exchange effects, the J values corresponding to the same k $(J=k\pm\frac{1}{2})$ have slightly different widths for moderate l_1: up to 10% difference for g states, significantly more for f states as shown below. However, for $l_1>5$, it appears that such effect is quite negligible. Similar information is provided by the relative variation between "exact" and long-range calculated widths, which is given in Table IV for the $6p_j24l_1[k]J$ states of Ba; this quantity roughly decreases by one order of magnitude for each unit of l_1.

TABLE II. Partial autoionization widths for the $6p_{3/2}24g$ $[k=\frac{9}{2}]$ $J=5$ state of barium (atomic units). In the fourth column one reads the autoionization probability for a given final ionic state, ejected-electron momentum l, and final momentum k'.

Threshold	l	k'	Probability	Probability (long range)
$6s_{1/2}$	5	$\frac{9}{2}$	6.088×10^{-7}	6.323×10^{-7}
	5	$\frac{11}{2}$	7.161×10^{-10}	0
	Total	$(6s_{1/2})$	6.095×10^{-7}	6.323×10^{-7}
$5d_{3/2}$	3	$\frac{9}{2}$	1.702×10^{-9}	1.108×10^{-8}
	5	$\frac{9}{2}$	8.214×10^{-8}	7.697×10^{-8}
	5	$\frac{11}{2}$	5.232×10^{-11}	0
	7	$\frac{11}{2}$	1.028×10^{-12}	0
	Total	$(5d_{3/2})$	8.389×10^{-8}	8.805×10^{-8}
$5d_{5/2}$	3	$\frac{9}{2}$	5.878×10^{-9}	1.696×10^{-9}
	5	$\frac{9}{2}$	9.412×10^{-7}	9.435×10^{-7}
	7	$\frac{9}{2}$	5.952×10^{-9}	6.063×10^{-9}
	3	$\frac{11}{2}$	1.186×10^{-8}	0
	5	$\frac{11}{2}$	1.224×10^{-10}	0
	7	$\frac{11}{2}$	3.483×10^{-13}	0
	Total	$(5d_{5/2})$	9.650×10^{-7}	9.512×10^{-7}
$6p_{1/2}$	4	$\frac{9}{2}$	6.149×10^{-7}	6.850×10^{-7}
	6	$\frac{11}{2}$	3.461×10^{-12}	0
	Total	$(6p_{1/2})$	6.149×10^{-7}	6.850×10^{-7}
	Total width		2.273×10^{-6}	2.357×10^{-6}

B. Dependence versus n_1

As is usual for unperturbed Rydberg series, the scaled autoionization width $n^3\Gamma$ varies smoothly with the energy $-1/n^2$. This function is plotted in Fig. 1 for $6p_{3/2}ng[k]J$ states in barium. One notices an abrupt increase of the probability between $n=8$ and $n=9$, which

TABLE III. Autoionization widths for the $6p_j 24l_1[k]J$ states in barium (atomic units). When written between two rows (e.g., for $6p_{3/2}24l_1=6$ $[k=\frac{11}{2}]$ states), the autoionization probability is the same for $J=k-\frac{1}{2}$ and $J=k+\frac{1}{2}$ at the table accuracy.

j	k	J	$l_1=4$	$l_1=5$	$l_1=6$	$l_1=7$	$l_1=8$	$l_1=9$	$l_1=10$
$\frac{3}{2}$	$l_1-\frac{3}{2}$	l_2-2	3.08×10^{-6}	4.97×10^{-7}	6.41×10^{-8}	6.36×10^{-9}			
							5.06×10^{-10}	3.56×10^{-11}	2.79×10^{-12}
	$l_1-\frac{3}{2}$	l_1-1	3.00×10^{-6}	4.99×10^{-7}	6.43×10^{-8}	6.37×10^{-9}			
	$l_1-\frac{1}{2}$	l_1-1	3.15×10^{-6}	6.29×10^{-7}					
					1.20×10^{-7}	2.48×10^{-8}	5.67×10^{-9}	1.33×10^{-9}	2.94×10^{-10}
	$l_1-\frac{1}{2}$	l_1	2.95×10^{-6}	6.24×10^{-7}					
	$l_1+\frac{1}{2}$	l_1	2.12×10^{-6}	4.53×10^{-7}	8.38×10^{-8}				
						1.71×10^{-8}	4.00×10^{-9}	9.67×10^{-10}	2.21×10^{-10}
	$l_1+\frac{1}{2}$	l_1+1	2.27×10^{-6}	4.57×10^{-7}	8.39×10^{-8}				
	$l_1+\frac{3}{2}$	l_1+1	3.21×10^{-6}	5.25×10^{-7}					
					1.11×10^{-7}	4.99×10^{-8}	2.73×10^{-8}	1.29×10^{-8}	5.04×10^{-9}
	$l_1+\frac{3}{2}$	l_1+2	2.90×10^{-6}	5.16×10^{-7}					
$\frac{1}{2}$	$l_1-\frac{1}{2}$	l_1-1	2.37×10^{-6}	4.40×10^{-7}					
					6.03×10^{-8}	6.28×10^{-9}	5.07×10^{-10}	3.23×10^{-11}	1.64×10^{-12}
	$l_1-\frac{1}{2}$	l_1	2.29×10^{-6}	4.38×10^{-7}					
	$l_1+\frac{1}{2}$	l_1	2.78×10^{-6}	4.74×10^{-7}					
					5.69×10^{-8}	5.17×10^{-9}	3.68×10^{-10}	2.09×10^{-11}	9.62×10^{-13}
	$l_1+\frac{1}{2}$	l_1+1	2.92×10^{-6}	4.79×10^{-7}					

is due to the opening of the $6p_{1/2}$ channels. Outside this region, the autoionization width may be accurately represented by a two-term formula $an^{-3}+bn^{-5}$, the coefficients depending on the various angular momenta. One also notices that the influence of the fine-structure transition is strongly dependent on the angular momentum k: the medium values $k=\frac{7}{2}$ and $\frac{9}{2}$ are much more sensitive to the $6p_{1/2}$ channel than the extremal ones.

C. Fine-structure effects

The influence of *fine-structure transitions* observed in Fig. 1 is also illustrated by Fig. 2, where the branching ratio for $(6p_{3/2}24l_1)$ $[k]J$ states of Ba to the $6p_{1/2}$ threshold is plotted as a function of l_1. It appears that for moderate l_1 (<7), the medium k values ($k=l_1\pm\frac{1}{2}$) correspond to the maximum fraction of slow electrons, while for higher l_1 the biggest k corresponds to the maximum percentage of such electrons. This can be understood by the following argument. The much lower branching ratio for $k=l_1-\frac{3}{2}$ may be attributed to angular factors and selection rules for quadrupolar transitions. Indeed, the $6p_{3/2}n_1l_1$ $[k=l_1-\frac{3}{2}]$ state autoionizes towards $6p_{1/2}\varepsilon l=l_1-2$ if k is conserved; conversely, if $k=l_1\pm\frac{1}{2}$, for the $6p_{1/2}$ threshold the ejected electron has $l=l_1$, while for $k=l_1+\frac{3}{2}$, the final l will be l_1+2. For example, the bound-free matrix elements $\langle \varepsilon l|r^{-3}|24g\rangle$ involved in long-range approximation are 3.346×10^{-6}, 8.547×10^{-5}, and 1.056×10^{-5} for $l=2,4$, and 6 respectively. As for dipolar transitions, there are propensity

TABLE IV. Relative variation of the $6p_j24l_1[k]J$ widths in barium between exact and long-range calculation. One reads the difference Γ(exact)/Γ(long range)-1 for the various states of the configuration. The exact values are the ones obtained within the present formalism with short-range effects (exchange and short-range contribution on the direct integral) included.

j	k	J	$l_1=3$	$l_1=4$	$l_1=5$	$l_1=6$	$l_1=7$
$\frac{3}{2}$	$l_1-\frac{3}{2}$	l_1-2	-2.87×10^{-1}	$+1.79\times10^{-2}$	-1.44×10^{-2}	-3.97×10^{-3}	-5.77×10^{-4}
	$l_1-\frac{3}{2}$	l_1-1	-1.27×10^{-1}	-1.08×10^{-2}	-9.19×10^{-3}	-1.62×10^{-3}	-2.06×10^{-4}
	$l_1-\frac{1}{2}$	l_1-1	-2.44×10^{-1}	-2.70×10^{-2}	-2.52×10^{-3}	-2.43×10^{-4}	-1.23×10^{-5}
	$l_1-\frac{1}{2}$	l_1	-4.07×10^{-1}	-8.90×10^{-2}	-1.09×10^{-2}	-8.65×10^{-4}	-4.37×10^{-5}
	$l_1+\frac{1}{2}$	l_1	-3.81×10^{-1}	-1.02×10^{-1}	-1.43×10^{-2}	-1.24×10^{-3}	-6.47×10^{-5}
	$l_1+\frac{1}{2}$	l_1+1	-1.98×10^{-1}	-3.54×10^{-2}	-4.46×10^{-3}	-3.62×10^{-4}	-1.81×10^{-5}
	$l_1+\frac{3}{2}$	l_1+1	$+9.14\times10^{-2}$	-1.11×10^{-1}	-3.88×10^{-3}	-3.10×10^{-4}	-7.15×10^{-6}
	$l_1+\frac{3}{2}$	l_1+2	-3.09×10^{-1}	-1.06×10^{-1}	-1.96×10^{-2}	-1.48×10^{-3}	-3.42×10^{-5}
$\frac{1}{2}$	$l_1-\frac{1}{2}$	l_1-1	-1.50×10^{-1}	-2.48×10^{-2}	-2.89×10^{-3}	-3.03×10^{-4}	-2.81×10^{-5}
	$l_1-\frac{1}{2}$	l_1	-2.05×10^{-1}	-5.58×10^{-2}	-8.63×10^{-3}	-1.02×10^{-3}	-1.04×10^{-4}
	$l_1+\frac{1}{2}$	l_1	-2.47×10^{-1}	-8.04×10^{-2}	-1.44×10^{-2}	-1.86×10^{-3}	-2.06×10^{-4}
	$l_1+\frac{1}{2}$	l_1+1	-1.61×10^{-1}	-3.23×10^{-2}	-4.64×10^{-3}	-5.51×10^{-4}	-5.84×10^{-5}

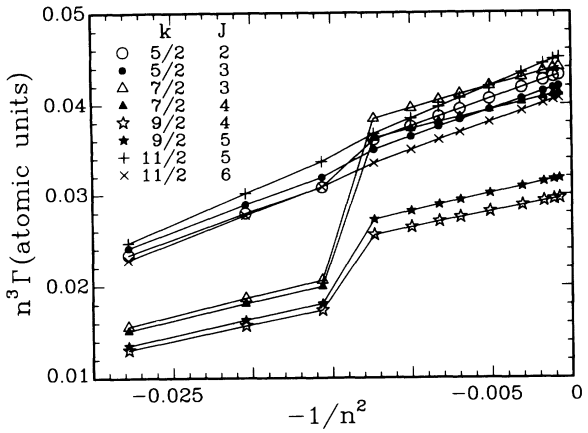

FIG. 1. Scaled autoionization width as a function of the energy. The quantity $n_1^3\Gamma$ for $6p_{3/2}n_1g[k]J$ states of barium is plotted vs the outer electron energy $-1/n_1^2$. The various symbols correspond to the different k and J values as specified. Data are plotted for $n_1=6$–12, 14, 18, 24, 30, and 36. The $6p_{1/2}$ channel is open if $n_1 \geq 9$.

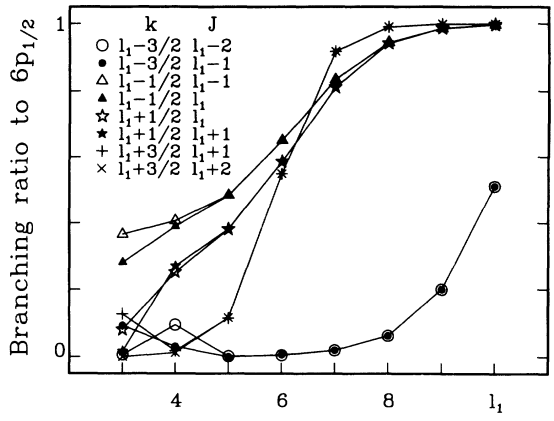

FIG. 2. Branching ratio to the $6p_{1/2}$ threshold. In the autoionization process of $6p_{3/2}24l_1[k]J$ states of barium, the fraction of ions left in the $6p_{1/2}$ state is plotted as a function of the momentum l_1. When this momentum is greater than 4, the data for $J=k\pm\frac{1}{2}$ almost coincide.

TABLE V. Autoionization widths of $5d_j24l_1[k]J$ states of barium (atomic units). When written between two rows, the autoionization width is the same for $J=k\pm\frac{1}{2}$ at the table accuracy. The radiative width is computed in hydrogen, accounting for the allowed transitions $24l_1 \rightarrow n'l_1\pm1$.

j	k	J	$l_1=3$	$l_1=4$	$l_1=5$	$l_1=6$	$l_1=7$	$l_1=8$	$l_1=9$	$l_1=10$
$\frac{5}{2}$	$l_1-\frac{5}{2}$	l_1-3	9.64×10^{-7}	3.93×10^{-8}	1.79×10^{-10}	7.51×10^{-11}				
							1.17×10^{-11}	2.06×10^{-12}	4.68×10^{-13}	1.24×10^{-13}
	$l_1-\frac{5}{2}$	l_1-2	2.32×10^{-6}	1.92×10^{-8}	4.55×10^{-10}	7.86×10^{-11}				
	$l_2-\frac{3}{2}$	l_1-2	1.17×10^{-6}	6.36×10^{-8}	1.32×10^{-8}					
						3.87×10^{-9}	1.27×10^{-9}	4.38×10^{-10}	1.50×10^{-10}	4.96×10^{-11}
	$l_1-\frac{3}{2}$	l_1-1	9.58×10^{-7}	6.02×10^{-8}	1.31×10^{-8}					
	$l_1-\frac{1}{2}$	l_1-1	6.30×10^{-7}	1.41×10^{-7}	2.73×10^{-8}					
						5.22×10^{-9}	1.03×10^{-9}	2.27×10^{-10}	5.83×10^{-11}	1.66×10^{-11}
	$l_1-\frac{1}{2}$	l_1	6.96×10^{-7}	1.42×10^{-7}	2.75×10^{-8}					
	$l_1+\frac{1}{2}$	l_1	1.50×10^{-6}	2.18×10^{-7}	3.35×10^{-8}					
						5.25×10^{-9}	8.23×10^{-10}	1.73×10^{-10}	7.27×10^{-11}	4.28×10^{-11}
	$l_1+\frac{1}{2}$	l_1+1	6.69×10^{-7}	1.92×10^{-7}	3.32×10^{-8}					
	$l_1+\frac{3}{2}$	l_1+1	1.21×10^{-7}	4.93×10^{-8}						
					1.94×10^{-8}	7.11×10^{-9}	2.42×10^{-9}	8.56×10^{-10}	3.60×10^{-10}	1.75×10^{-10}
	$l_1+\frac{3}{2}$	l_1+2	8.19×10^{-8}	5.13×10^{-8}						
	$l_1+\frac{5}{2}$	l_1+2	5.89×10^{-7}	1.19×10^{-7}						
					6.50×10^{-8}	2.53×10^{-8}	7.50×10^{-9}	1.92×10^{-9}	5.50×10^{-10}	2.25×10^{-10}
	$l_1+\frac{5}{2}$	l_1+3	1.10×10^{-7}	1.17×10^{-7}						
$\frac{3}{2}$	$l_1-\frac{3}{2}$	l_1-2	1.17×10^{-7}	2.71×10^{-10}	2.15×10^{-10}	4.78×10^{-11}	6.72×10^{-12}			
								8.05×10^{-13}	8.36×10^{-14}	7.50×10^{-15}
	$l_1-\frac{3}{2}$	l_1-1	1.94×10^{-7}	9.57×10^{-9}	6.72×10^{-11}	4.44×10^{-11}	6.69×10^{-12}			
	$l_1-\frac{1}{2}$	l_1-1	5.62×10^{-7}	1.56×10^{-7}	2.79×10^{-8}					
						4.65×10^{-9}	7.21×10^{-10}	1.00×10^{-10}	1.22×10^{-11}	1.29×10^{-12}
	$l_1-\frac{1}{2}$	l_1	9.26×10^{-7}	1.65×10^{-7}	2.80×10^{-8}					
	$l_1+\frac{1}{2}$	l_1	4.36×10^{-7}	8.54×10^{-8}	1.62×10^{-8}	2.93×10^{-9}				
							4.82×10^{-10}	7.04×10^{-11}	8.91×10^{-12}	9.67×10^{-13}
	$l_1+\frac{1}{2}$	l_1+1	2.34×10^{-7}	7.94×10^{-8}	1.61×10^{-8}	2.92×10^{-9}				
	$l_1+\frac{3}{2}$	l_1+1	6.57×10^{-8}	8.05×10^{-8}						
					5.02×10^{-8}	2.19×10^{-8}	7.09×10^{-9}	1.77×10^{-9}	3.48×10^{-10}	5.47×10^{-11}
	$l_1+\frac{3}{2}$	l_1+2	7.69×10^{-8}	8.10×10^{-8}						
Radiative rate		$(24l_1)$	1.67×10^{-12}	1.00×10^{-12}	6.67×10^{-13}	4.74×10^{-13}	3.54×10^{-13}	2.74×10^{-13}	2.18×10^{-13}	1.77×10^{-13}

rules on quadrupolar elements which state that, for moderate l_1 (in the present case less than 8), the transition $l_1 \rightarrow l_1$ is significantly more probable than $l_1 \rightarrow l_1+2$ which is in turn more probable than $l_1 \rightarrow l_1-2$. For higher l_1, the ordering changes to (l_1+2, l_1, l_1-2) and accordingly, the maximum autoionization probability towards $6p_{1/2}$ is obtained for $k=l_1+\frac{3}{2}$. More significantly, it appears that *in the large-l limit, the fine-structure transition is the favored autoionization decay channel,* whatever the angular momenta k or J. This statement is corroborated by the observations on the $6p_{3/2}nh$ series by Bente and Hogervorst [7].

D. Quadrupolar transitions

As another example, the $5d_j24l_1[k]J$ autoionization widths of barium are detailed in Table V. Such states only decay by quadrupolar transitions to the $5d_{3/2}$ threshold if permitted and to the $6s_{1/2}$ threshold. Thus specific stability properties are expected. Besides, the valence-electron wave function has a small radial extension, making the nonoverlap hypothesis generally easy to comply with. Comparing these results to those concerning $6p_j24l_1$ states in Table III, one notices that the present probabilities are one or a few orders of magnitude smaller for moderate l_1, but for large l_1 the figures are not very different. As stated above, this can be explained by the quadrupolar transitions that become dominant for large l_1. Once again, one observes a strong variation of the probabilities with k, according to the possible value for the final angular momentum; for example, the lifetimes of $5d_{5/2}24l_1=7$ range from 2.1 μs ($k=l_1-\frac{5}{2}$) to 3.2 ns ($k=l_1+\frac{5}{2}$) and if $l_1=10$ from 200 μs to 110 ns. In the present case, long autoionization lifetimes may be observable since such states hardly decay radiatively. The $5d_{5/2,3/2}$ lifetimes in Ba^+ are 37 s and 84 s, respectively [21,29]; more probable is the radiative decay of the *outer* electron which, treating the inner electron as spectator and the outer one as hydrogenic, occurs in 140 μs for $l_1=10$ and 14 μs for $l_1=3$ (last row of Table V). Except for the minimum k value, autoionization is still more probable than radiative decay even for $l_1=10$. This demonstrates the interest for studying such long-lived doubly excited states. Some experimental data are available for the $5dnf$ [13] and $5dng$ [30] series, the first one being discussed in the next section.

E. Computation in strontium

Similar computations have been performed in strontium for $5p_{3/2}24l$ and $5p_{1/2}24l$ states. The results are presented in Figs. 3 and 4. The general properties observed on barium still hold; one will notice that probabilities are a little larger because the ejected electron is of smaller energy. The change in slope for the $5p_{3/2}24l_1$ $[k=l_1+\frac{3}{2}]$ autoionization probability for $l_1=7$ can be attributed to the fine-structure contribution which becomes dominant for this l_1 value. Besides, including for the highest l_1 considered (10), the $4d_{5/2}$-threshold contribution cannot be ignored in the $5p_{3/2}24l_1$ autoionization,

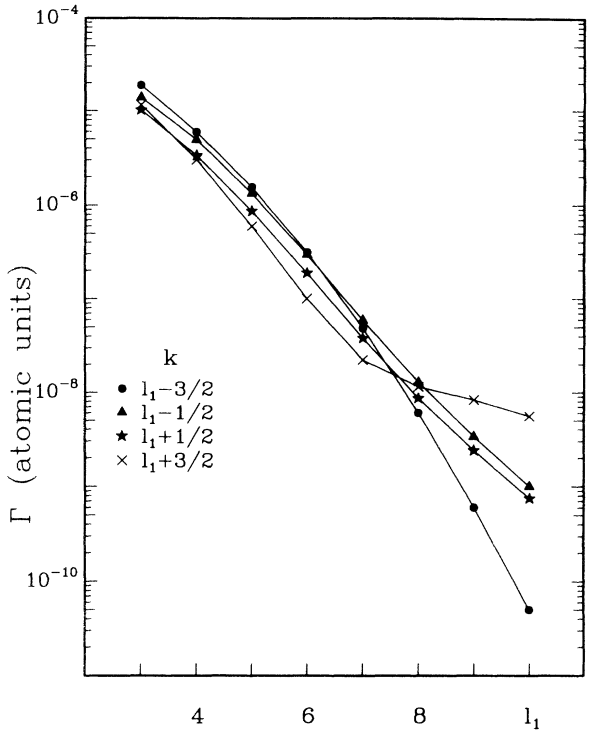

FIG. 3. Autoionization width for the $5p_{3/2}24l_1[k]$ states of strontium (atomic units). The width is plotted as a function of l_1 for the $J=k+\frac{1}{2}$ states. The data points are indistinguishable from the $J=k-\frac{1}{2}$ points at the drawing accuracy.

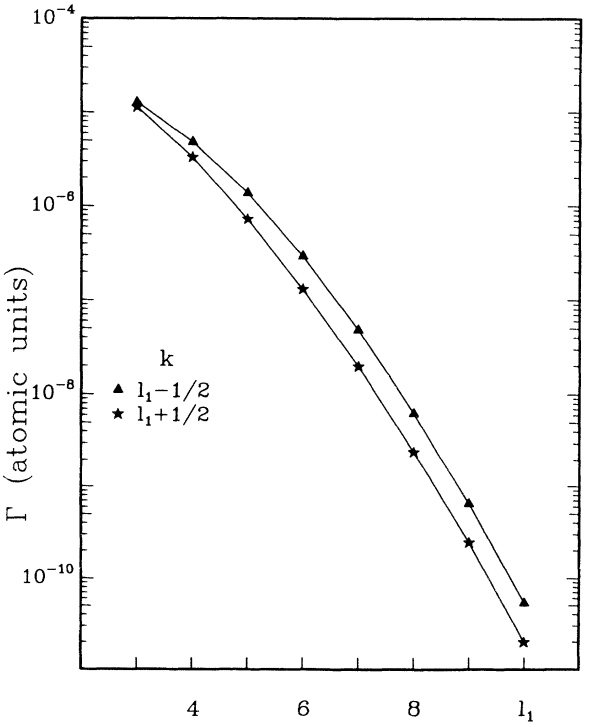

FIG. 4. Autoionization width for the $5p_{1/2}24l_1[k]$ states of strontium (atomic units). See comments about Fig. 3.

it remains the dominant channel for the lowest k values ($l_1-\frac{3}{2}$). For these states, the decrease of autoionization probability with l_1 is slower than for corresponding states in barium because the ejected electron is less energetic: $\varepsilon(4d_{5/2})=4.33\times10^{-2}$ a.u. and $\varepsilon(5p_{1/2})=2.78\times10^{-3}$ a.u. in strontium versus $\varepsilon(5d_{5/2})=7.33\times10^{-2}$ a.u. and $\epsilon(6p_{1/2})=6.84\times10^{-3}$ a.u. in barium. When k varies, the widths for $5p_{3/2}24l_1=10[k]$spread over two orders of magnitude in strontium against more than three in barium. For energetic reasons, as well, the autoionization widths of $5p_{1/2}24l_1[k]$ states decrease more slowly in strontium than in barium.

V. COMPARISON WITH EXPERIMENTAL DATA

Really quantitative data on autoionization width for large-l states are rather scarce, so few significant checks of the present formalism can be done. Some indications about its validity range will be given here.

A first comparison with experiment can be done using data by Jaffe *et al.* [3]. The measured values for $6p_{3/2}24g[k]$ $J=5$ are 0.87 and 0.69 cm^{-1} for $k=\frac{9}{2}$ and $\frac{11}{2}$, respectively. As shown in Table III, the present model gives 0.499 and 0.705 cm^{-1}. The computed branching ratio to the $6p_{1/2}$ threshold is 0.271 and 0.018, respectively. As discussed in the previous section, the fine-structure transition has a maximum probability when a $\Delta l=0$ transition is allowed, i.e., when $k=l_1\pm\frac{1}{2}$. In the present case, without considering fine-structure transition, the autoionization width would be 0.36 and 0.69 cm^{-1} for $k=\frac{9}{2}$ and $\frac{11}{2}$, increasing the global disagreement with experiment. However, it appears that fine-structure contribution is underestimated by the present treatment.

The $6p_j24f[k]J$ autoionization widths in barium are listed in Table VI. For these states, a detailed experimental analysis has been done by Abutaleb *et al.* [15]. A R-matrix and multichannel quantum defect theory (MQDT) computation has been performed by Telmini, Aymar, and Lecomte [31] and agrees fairly well with the measured data. There also exists a single-configuration computation and measurements on $6p_{1/2}nf$ by Wang, Story, and Cooke [32]. The present large-l analysis is pushed a little beyond its limit of applicability for f states, since their inner classical turning point [$r_-(24f)=6.03$ a.u.] falls inside the classically allowed region for the valence electron [$r_+(6p_{1/2})=6.72$ a.u., $r_+(6p_{3/2})=6.94$ a.u.]. Even more significant is the high value of the scaled autoionization width $n^3\Gamma$, usually greater than 0.1 including for the $6p_{1/2}24f$ states, which corresponds to an autoionization probability close to 1 per orbiting time. However, we get at least a qualitative picture. As a rule, the calculated widths are about one half of those deduced by Abutaleb *et al.* from their measurements by a MQDT analysis. The long-range approximation, the results of which are mentioned in the experimental paper, is closer to the measurements since, as shown above, exchange effects generally tend to decrease the probabilities. From Tables IV and VI one observes that short-range effects are far from negligible since the computed widths of $J=k\pm\frac{1}{2}$ may significantly differ and differ also from the long-range approximation. In spite of discrepancies in absolute values, one must notice from Table VI that the *relative* values of the probabilities are fairly well reproduced. For example, the experimental ratio $\Gamma(6p_j24f[k]$ $J=k+\frac{1}{2})/\Gamma(6p_j24f[k]$ $J=k-\frac{1}{2})$ is 0.64(23), 1.50(21), 0.72(16), 1.06(17), 1.06(14) for $(j,k)=(\frac{3}{2},\frac{5}{2})$, $(\frac{3}{2},\frac{7}{2})$, $(\frac{3}{2},\frac{9}{2})$, $(\frac{1}{2},\frac{5}{2})$, and $(\frac{1}{2},\frac{7}{2})$, respectively, the numbers in parentheses being the uncertainty in the last quoted digits; the corresponding numbers within the present formalism are 0.784, 1.30, 0.633, 0.935, and 1.11, all within error bars and significantly different from 1, which would be the long-range result. From the last column of Table VI one notices a roughly constant factor of $\frac{1}{2}$ between theory and experiment. As an exception, a special mention has to be made for the $6p_{3/2}24f$ $[k=\frac{5}{2}]$ states which, from Table VI, are those for which the branching ratio to the $6p_{1/2}$ threshold is maximum (0.366 and 0.281 for $J=2$ and 3, respectively). Once again, one observes that the present theory systematically underestimates the contribution of such quadrupolar transitions. A possible explanation is the following: fine-structure transitions are possible through the quadrupolar term of the interaction $1/r_{12}$ considered at first order, but also through the dipolar term of the same interaction considered at second order. Probably, such a second-order contribution is not negligible in the present case. This situation also prevails when one calculates the energy position of singly excited states of helium [23] or doubly excited large-l states [8]. Accounting for such corrections, one will probably get for the $k=\frac{5}{2}$ states a computed-to-measured-width ratio similar to the one for other k values. Considering second-order corrections amounts to the use of wave functions with correlated electrons.

A better check of the present results is provided by measurements on $5d_jnf$ levels since the wave function overlap is then smaller. Including polarization terms in the potential [21], one computes the classical outer turning points $r_+(5d_{3/2})=3.89$ and $r_+(5d_{5/2})=3.95$ a.u. Above the $5d_{3/2}$ threshold, the reported scaled half width at half maximum (HWHM) for the series labeled $(5d_{5/2}nf_-)$ $J=5$ is 13 000 GHz [13], that is, a full width at half maximum (FWHM) equal to 2.9×10^{-7} a.u. if n is 24. Assuming the value $k=\frac{9}{2}$ can be attributed to this series [33], this is greater than the calculated value in Table V (8.2×10^{-8}). In the present case, the long-range approximation would give a very different result (2.1×10^{-7}). This does not mean that exchange effects must be ignored in the present case; as shown below and as apparent from Table V, the other $J=5$ level has a much larger width and if the true coupling is not jk but some intermediate coupling, as may be suspected for such low-l states, the present calculated width will probably be increased by this k mixing. Besides, a previously published value [33] was 5400 GHz for this same scaled HWHM, which gives a width (FWHM) of 1.2×10^{-7} a.u. for $n=24$ in much better agreement with the Table V value. On the other hand, the scaled half width of the other $J=5$ series, labeled $5d_{5/2}nf_+$ by the authors [13,33] changes from 650 to 35 000 GHz when the $5d_{3/2}$ threshold is crossed. For $n=24$, the corresponding

TABLE VI. Autoionization widths of $6p_j 24f[k]J$ states in barium (atomic units). The experimental data are from Abutaleb *et al.* [15], the width of $6p_{3/2}24f\ [k=\frac{3}{2}]\ J=2$ being unavailable. The branching ratio to $6p_{1/2}$ is a value computed within the present formalism including exchange. The numbers between parentheses are experimental errors in terms of the last quoted digit. From its definition, the long-range width is the same for $J=k\pm\frac{1}{2}$.

			Autoionization probability (a.u.)			Branching	Obs.:calc.
j	k	J	Experiment	This work	Long range	ratio to $6p_{1/2}$	ratio
$\frac{3}{2}$	$\frac{3}{2}$	1	$2.0(2)\times10^{-5}$	1.11×10^{-5}		0.006 47	1.8(2)
					1.56×10^{-5}		
	$\frac{3}{2}$	2	—	1.37×10^{-5}		0.093 1	
	$\frac{5}{2}$	2	$4.7(14)\times10^{-5}$	1.27×10^{-5}		0.366	3.7(11)
					1.68×10^{-5}		
	$\frac{5}{2}$	3	$3.0(6)\times10^{-5}$	9.94×10^{-6}		0.281	3.0(6)
	$\frac{7}{2}$	3	$1.2(1)\times10^{-5}$	6.20×10^{-6}		0.080 7	1.9(2)
					1.00×10^{-5}		
	$\frac{7}{2}$	4	$1.8(2)\times10^{-5}$	8.04×10^{-6}		0.170	2.2(2)
	$\frac{9}{2}$	4	$3.2(6)\times10^{-5}$	1.73×10^{-5}		0.127	1.9(3)
					1.58×10^{-5}		
	$\frac{9}{2}$	5	$2.3(3)\times10^{-5}$	1.09×10^{-5}		1.44×10^{-5}	2.1(3)
$\frac{1}{2}$	$\frac{5}{2}$	2	$1.7(2)\times10^{-5}$	9.16×10^{-6}			1.9(2)
					1.08×10^{-5}		
	$\frac{5}{2}$	3	$1.8(2)\times10^{-5}$	8.57×10^{-6}			2.1(2)
	$\frac{7}{2}$	3	$1.6(1)\times10^{-5}$	1.03×10^{-5}			1.5(1)
					1.37×10^{-5}		
	$\frac{7}{2}$	4	$1.7(2)\times10^{-5}$	1.15×10^{-5}			1.5(2)

FWHM is 7.7×10^{-7} a.u., in good agreement with the computed value (5.89×10^{-7}) if we assign $k=\frac{11}{2}$ to this series. Here again, the long-range approximation would be far from sufficient, giving 1.35×10^{-7} a.u. A study of the theoretical branching ratio shows that the preferred final state is then $5d_{3/2}\varepsilon f\ [k=\frac{9}{2}]$; this agrees with the observation of the prevalence of the fine-structure transition and provides a situation where a k-changing transition may be dominant. Computations have also been performed in the jj-coupling scheme. The $(5d_{5/2}24f_j)\ J=5$ widths are 2.04×10^{-7}, 4.67×10^{-7} for $j=\frac{7}{2}$ and $\frac{5}{2}$, respectively; the former value roughly agrees with the "f_-" experimental data but the latter is in stronger disagreement with the "f_+" data than the result in the jk coupling; here the correct coupling is probably intermediate. The present analysis proves that short-range effects may be quite important even when both electron wave functions do not overlap; it also stresses the necessity to define correctly the coupling scheme.

In order to emphasize the influence of higher multipoles, it is interesting to quote the results in "double circular states" $4f5g\ [J=2]$ of barium by Jones, Fu, and Gallagher [19]. A direct comparison with their data is not easy because the observed levels are labeled in the jj-coupling scheme and because the corresponding widths have to be extracted from the figures. The $4f_{5/2}5g_{7/2}$ width (FWHM) is about 6 cm^{-1}, the $4f_{5/2}5g_{9/2}$ peak is small, and its width is very difficult to estimate (perhaps 9 cm^{-1}). The long-range formalism gives 18 and 8.5 cm^{-1} for $k=\frac{5}{2}$ and $\frac{3}{2}$ which, considering the bigger coefficient in the transformation matrix, may be assigned to the jj-coupled states $f_{5/2}g_{7/2}$ and $f_{5/2}g_{9/2}$, respectively. The favored thresholds are $7s_{1/2}$ and $5d_{5/2}$, respectively, so the $k=\frac{5}{2}$ level decays mainly by octupolar transition. However, if one computes short-range effects, one gets quite different figures (2.6 and 20 cm^{-1} for $k=\frac{5}{2}$ and $\frac{3}{2}$, respectively). No quantitative conclusion should be drawn from this comparison. The short-range effects are uneasy to evaluate correctly since $4f$ states in barium II are very sensitive to the double-well structure of the potential [34]; besides, as we stated above concerning quadrupolar transitions, higher-order effects should be considered when octupolar terms are involved. Similar conclusions arise when considering $4f_{7/2}5g$ states. The estimated experimental widths are 10 and 16 cm^{-1} for $g_{7/2}$ and $g_{9/2}$ electrons while, assigning again the k value through the maximum weight in the transformation matrix, one gets 16 and 6 cm^{-1} for $k=\frac{5}{2}$ and $\frac{3}{2}$, respectively. Here again, inclusion of short-range terms changes significantly these figures in 2.6 and 12 cm^{-1}. Clearly additional work is desirable both theoretically—in addition to the above-mentioned special character of the $4f$ level in barium II, the $4f$ threshold is close to the $6d$ threshold, so configuration mixing is certainly very important—and experimentally to get more accurate lifetimes and to assign correctly the k angular momentum. However, it turns out that, including quadrupolar and octupolar terms, one is able to get at least an order of magnitude of the $4f5g$ widths, while consideration of the dipolar term only is far from sufficient [19]. Moreover, as was stated previously [19], the $4f$ and$5g$ classically allowed regions do not overlap; the present first-order com-

putation of short-range effects proves that such condition is not sufficient to ignore exchange.

VI. CONCLUSION

The present work is an exact computation of autoionization widths of large-l Rydberg states within first-order perturbation theory, in the framework of jk coupling. As in the long-range formulation, one observes a rapid decrease of autoionization probability with l_1. But this statement needs to be tempered: while for the lowest k value ($l_1-\frac{3}{2}$) the $6p_{3/2}n_1l_1[k]$ width in barium roughly decreases by one order of magnitude for each unit of l_1, this is no longer true for the other k values, and especially the highest one ($l_1+\frac{3}{2}$), its lifetime changing from 0.49 ns for $l_1=7$ to 4.8 ns for $l_1=10$. In the latter case, the computed lifetime of ($6p_{3/2}24l_1=10$) [$k=\frac{17}{2}$] is three orders of magnitude longer (8.7 μs). This emphasizes the need to account properly for the coupling scheme in the doubly excited atom. Besides, it is remarkable that in the large-l limit, the fine-structure contribution tends to be the only significant one. While fine-structure effects tends to increase dramatically with the angular momentum l_1, exchange effects also considered here rapidly decrease with l_1. An indication of their influence is given by the relative variation of the width between two states of a pair ($J=k\pm\frac{1}{2}$ for a given k). Concerning the $6p_j24f[k]$ states of barium, the computed relative variation agrees with experimental data by Abutaleb *et al.*, while the absolute computed widths are about twice the measured ones. For g states, one expects the exchange effects not to affect the widths by more than 10 and 2% for h states, respectively. So the present work defines quantitatively the validity domain of the long-range formalism previously used. Some limitations concerning its applicability for quadrupolar transitions have been emphasized. Clearly, this single-configuration approach is not relevant in regions where series perturbations are important. Possible refinements of the formalism, involving the accounting for second-order effects, will be considered in a forthcoming paper.

ACKNOWLEDGMENTS

The author gratefully acknowledges constant encouragement and helpful advice from Dr. F. Gounand. He is also indebted to Dr. B Carré, Dr. G Spiess, and Dr. J. Pascale for fruitful discussions.

APPENDIX: ANGULAR FACTOR FOR THE EXCHANGE AMPLITUDE IN jk COUPLING

The exchange amplitude in jk coupling is written as

$$\mathcal{A}_e=\sum_{t\geq 0}\langle \varepsilon l,n_0l_0j_0|r_<^t/r_>^{t+1}|n_2l_2j_2,n_1l_1\rangle \times \begin{pmatrix} l & t & l_2 \\ 0 & 0 & 0 \end{pmatrix}\begin{pmatrix} l_0 & t & l_1 \\ 0 & 0 & 0 \end{pmatrix}[l,l_1]^{1/2}X\ , \tag{A1a}$$

with

$$X=(-1)^{J+t+1}[l_0,l_2,j_0,j_2,k,k']^{1/2} \times \begin{Bmatrix} \frac{1}{2} & l_2 & l & k' \\ j_2 & t & j_0 & J \\ k & l_1 & l_0 & \frac{1}{2} \end{Bmatrix}, \tag{A1b}$$

where the notation

$$[a,b,\dots]=(2a+1)(2b+1)\dots \tag{A2}$$

has been used. The $12j$ symbol of the second kind is defined as [24]

$$\begin{bmatrix} j_1 & j_2 & j_3 & j_4 \\ l_1 & l_2 & l_3 & l_4 \\ k_1 & k_2 & k_3 & k_4 \end{bmatrix}=\sum_g(-1)^S(2g+1)\begin{Bmatrix} j_1 & k_1 & g \\ k_2 & j_2 & l_1 \end{Bmatrix}\begin{Bmatrix} j_2 & k_2 & g \\ k_3 & j_3 & l_2 \end{Bmatrix}\begin{Bmatrix} j_3 & k_3 & g \\ k_4 & j_4 & l_3 \end{Bmatrix}\begin{Bmatrix} j_4 & k_4 & g \\ k_1 & j_1 & l_4 \end{Bmatrix}, \tag{A3a}$$

with

$$S=\sum_{i=1}^{4}(j_i+k_i+l_i)\ . \tag{A3b}$$

Graphically, this symbol may be figured as a hexahedron (say, a cube) in the same way a $6j$ symbol may be represented as a tetrahedron.

For the considered symbols, since two momenta are equal to $\frac{1}{2}$, one gets, using the definition (A3) and the known values for $6j$ symbols with one momentum equal to $\frac{1}{2}$ [35], four different expressions according to the k and k' values. With the notations

$$\epsilon=2(j_2-l_2)\ , \tag{A4a}$$

$$\epsilon'=2(j_0-l_0)\ , \tag{A4b}$$

$$s=l_1+l_2+1\ , \tag{A4c}$$

$$s'=l+l_0+1\ , \tag{A4d}$$

$$d = l_1 - l_2 \ , \tag{A4e}$$

$$d' = l - l_0 \ , \tag{A4f}$$

one writes the following angular factors. For $k = J - \frac{1}{2}, k' = J + \frac{1}{2}$,

$$X = \frac{(-1)^{j_2 + l_0 + 1/2}}{2J+1} \{(s - \epsilon J)(J + \epsilon d)[s' + \epsilon'(J+1)](J + 1 - \epsilon' d')\}^{1/2} \begin{Bmatrix} l_1 & l_2 & J \\ l & l_0 & t \end{Bmatrix} , \tag{A5a}$$

for $k = J + \frac{1}{2}, k' = J - \frac{1}{2}$,

$$X = \frac{(-1)^{j_0 + l_2 + 1/2}}{2J+1} \{[s + \epsilon(J+1)](J + 1 - \epsilon d)(s' - \epsilon' J)(J + \epsilon' d')\}^{1/2} \begin{Bmatrix} l_1 & l_2 & J \\ l & l_0 & t \end{Bmatrix} , \tag{A5b}$$

for $k = k' = J - \frac{1}{2}$,

$$X = \frac{(-1)^{l_2 + l_0}}{2J} [(s + \epsilon J)(J - \epsilon d)(s' + \epsilon' J)(J - \epsilon' d')]^{1/2} \begin{Bmatrix} l_1 & l_2 & J-1 \\ l & l_0 & t \end{Bmatrix}$$
$$+ \frac{(-1)^{j_2 + j_0 - 1}}{2J(2J+1)} [(s - \epsilon J)(J + \epsilon d)(s' - \epsilon' J)(J + \epsilon' d')]^{1/2} \begin{Bmatrix} l_1 & l_2 & J \\ l & l_0 & t \end{Bmatrix} , \tag{A5c}$$

and for $k = k' = J + \frac{1}{2}$,

$$X = \frac{(-1)^{l_2 + l_0 - 1}}{(2J+1)(2J+2)} \{(s + \epsilon(J+1)](J + 1 - \epsilon d)[s' + \epsilon'(J+1)](J + 1 - \epsilon' d')\}^{1/2} \begin{Bmatrix} l_1 & l_2 & J \\ l & l_0 & t \end{Bmatrix}$$
$$+ \frac{(-1)^{j_2 + j_0 - 1}}{(2J+2)} \{[s - \epsilon(J+1)](J + 1 + \epsilon d)[s' - \epsilon'(J+1)](J + 1 + \epsilon' d')\}^{1/2} \begin{Bmatrix} l_1 & l_2 & J+1 \\ l & l_0 & t \end{Bmatrix} . \tag{A5d}$$

In this work, a computer program has been used to get these elements in terms of square roots of rational numbers. In this way, the angular factors are obtained with the best available numerical accuracy, i.e., without any rounding due to difference effects in computation of a sum.

[1] U. Fano, Rep. Prog. Phys. **46**, 97 (1983); C. D. Lin, Adv. At. Mol. Phys. **22**, 77 (1986); D. Wintgen, K. Richter, and G. Tanner, Chaos **2**, 19 (1992).

[2] W. Sandner, Comments At. Mol. Phys. **20**, 171 (1987); W. Hogervorst, *ibid.* **29**, 245 (1993).

[3] S. M. Jaffe, R. Kachru, H. B. van Linden van den Heuvell, and T. F. Gallagher, Phys. Rev. A **32**, 1480 (1985).

[4] R. R. Jones and T. F. Gallagher, Phys. Rev. A **38**, 2846 (1988).

[5] M. Poirier, Phys. Rev. A **38**, 3484 (1988).

[6] H. Van Regemorter, J. Phys. B **23**, 1797 (1990).

[7] E. A. J. M. Bente and W. Hogervorst, J. Phys. B **23**, 1403 (1990).

[8] L. Pruvost, P. Camus, J.-M. Lecomte, C. R. Mahon, and P. Pillet, J. Phys. B **24**, 4723 (1991).

[9] P. Camus, J.-M. Lecomte, C. R. Mahon, P. Pillet, and L. Pruvost, J. Phys. II **2**, 715 (1992).

[10] W. Sandner, R. Kachru, K. A. Safinya, F. Gounand, W. E. Cooke, and T. F. Gallagher, Phys. Rev. A **27**, 1717 (1983).

[11] R. Kachru, N. H. Tran, H. B. van Linden van den Heuvell, and T. F. Gallagher, Phys. Rev. A **30**, 667 (1984).

[12] L. Pruvost, A. Bolovinos, P. Camus, J.-M. Lecomte, and P. Pillet, J. Phys. B **23**, L95 (1990).

[13] E. A. J. M. Bente and W. Hogervorst, J. Phys. B **22**, 2679 (1989).

[14] F. Roussel, M. Chéret, L. Chen, T. Bolzinger, G. Spiess, J. Hare, and M. Gross, Phys. Rev. Lett. **65**, 3112 (1990).

[15] M. Abutaleb, R. J. de Graaf, W. Ubachs, and W. Hogervorst, Phys. Rev. A **44**, 4187 (1991).

[16] V. N. Ostrovsky and N. V. Prudov, J. Phys. B **26**, L263 (1993).

[17] P. Camus, S. Cohen, L. Pruvost, and A. Bolovinos, Phys. Rev. A **48**, R9 (1993).

[18] L. Chen, M. Chéret, M. Poirier, F. Roussel, T. Bolzinger, and G. Spiess, J. Phys. II **2**, 701 (1992).

[19] R. R. Jones, Panming Fu, and T. F. Gallagher, Phys. Rev. A **44**, 4260 (1991).

[20] S. I. Nikitin and V. N. Ostrovsky, J. Phys. B **13**, 1961 (1980).

[21] M. Poirier, Z. Phys. D **25**, 117 (1993).

[22] R. D. Cowan, *The Theory of Atomic Structure and Spectra* (University of California Press, Berkeley, 1981).

[23] H. A. Bethe and E. E. Salpeter, *Quantum Mechanics of One- and Two-Electron Atoms* (Plenum, New York, 1977).

[24] D. A. Varshalovich, A. N. Moskalev, and V. K. Khersonskii, *Quantum Theory of Angular Momentum* (World Scientific, Singapore, 1988).

[25] C. Froese, Can. J. Phys. **41**, 1895 (1963).

[26] W. R. Johnson, D. Kolb, and K. N. Huang, At. Data Nucl. Data Tables **28**, 33 (1983); J.-P. Desclaux, *ibid.* **12**, 311 (1973).

[27] M. J. Seaton, Comput. Phys. Commun. **25**, 87 (1982).

[28] P. H. Butler, P. E. H. Minchin, and B. G. Wybourne, At. Data **3**, 153 (1971).
[29] C. Guet and W. R. Johnson, Phys. Rev. A **44**, 1531 (1991).
[30] E. A. J. M. Bente and W. Hogervorst, Z. Phys. D **14**, 119 (1989).
[31] M. Telmini, M. Aymar, and J.-M. Lecomte, J. Phys. B **26**, 233 (1993).
[32] X. Wang, J. G. Story, and W. E. Cooke, Phys. Rev. A **43**, 3535 (1991).
[33] E. A. J. M. Bente and W. Hogervorst, Phys. Rev. A **36**, 4081 (1987).
[34] M. Goeppert-Mayer, Phys. Rev. **60**, 184 (1941); A. R. P. Rau and U. Fano, *ibid.* **167**, 7 (1968); D. C. Griffin, R. D. Cowan, and K. L. Andrew, Phys. Rev. A **3**, 1233 (1971); L. J. Curtis and P. S. Ramanujam, J. Opt. Soc. Am. **71**, 1315 (1981); J.-P. Connerade, J. Phys. B **24**, L109 (1991).
[35] A. R. Edmonds, *Angular Momentum in Quantum Mechanics* (Princeton University Press, Princeton, NJ, 1968).